

Wing Rotation and the Aerodynamic Basis of Insect Flight

Michael H. Dickinson,^{1*} Fritz-Olaf Lehmann,² Sanjay P. Sane¹

The enhanced aerodynamic performance of insects results from an interaction of three distinct yet interactive mechanisms: delayed stall, rotational circulation, and wake capture. Delayed stall functions during the translational portions of the stroke, when the wings sweep through the air with a large angle of attack. In contrast, rotational circulation and wake capture generate aerodynamic forces during stroke reversals, when the wings rapidly rotate and change direction. In addition to contributing to the lift required to keep an insect aloft, these two rotational mechanisms provide a potent means by which the animal can modulate the direction and magnitude of flight forces during steering maneuvers. A comprehensive theory incorporating both translational and rotational mechanisms may explain the diverse patterns of wing motion displayed by different species of insects.

Insects were the first animals to evolve active flight and remain unsurpassed in many aspects of aerodynamic performance and maneuverability. Among insects, we find animals capable of taking off backwards, flying sideways, and landing upside down (1). While such complex aerial feats involve many physiological and anatomical specializations that are poorly understood, perhaps the greatest puzzle is how flapping wings can generate enough force to keep an insect in the air. Conventional aerodynamic theory is based on rigid wings moving at constant velocity. When insect wings are placed in a wind tunnel and tested over the range of air velocities that they encounter when flapped by the animal, the measured forces are substantially smaller than those required for active flight (2). Thus, something about the complexity of the flapping motion increases the lift produced by a wing above and beyond that which it could generate at constant velocity or that can be predicted by standard aerodynamic theory.

The failure of conventional steady-state theory has prompted the search for unsteady mechanisms that might explain the high forces produced by flapping wings (3, 4). The wingstroke of an insect is typically divided into four kinematic portions: two translational phases (upstroke and downstroke), when the wings sweep through the air with a high angle of attack, and two rotational phases (pronation and supination), when the wings

rapidly rotate and reverse direction. The unsteady mechanisms that have been proposed to explain the elevated performance of insect wings typically emphasize either the translational or rotational phases of wing motion (3, 5–8). The first unsteady effect to be identified was a rotational mechanism termed the “clap and fling,” a close apposition of the two wings preceding pronation that hastens the development of circulation during the downstroke (9). Although the clap and fling may be important, especially in small species, it is not used by all insects (10) and thus cannot represent a general solution to the enigma of force production. Recent studies using real and dynamically scaled models of hawk moths suggest that a translational mechanism, termed “delayed stall,” might explain how insect wings generate such large forces (11). At high angles of attack, a flow structure forms on the leading edge of a wing that can transiently generate circulatory forces in excess of those supported under steady-state conditions (7). On flapping wings, this leading edge vortex is stabilized by the presence of axial flow, thereby augmenting lift throughout the downstroke (5, 11). Several additional unsteady mechanisms have been proposed (6), mostly based on wing rotation, but recent studies have found little or no evidence for their use by insects (11). Despite this lack of evidence, it is unlikely that insects rely solely on translational mechanisms to fly. Whereas delayed stall might account for enough lift to keep an insect aloft, it cannot easily explain how many insects can generate aerodynamic forces that exceed twice their body weight while carrying loads (10).

One persistent obstacle in the search for additional unsteady mechanisms is the difficulty in directly measuring the forces produced by a flapping insect (12). In order to further explore the aerodynamic basis of in-

sect flight, we built a dynamically scaled model of the fruit fly, *Drosophila melanogaster*, equipped with sensors at the base of one wing capable of directly measuring the time course of aerodynamic forces (Fig. 1A). The forces generated by a pattern of wing motion based on *Drosophila* kinematics (13) are shown in Fig. 1, C through G. Both the magnitude and the orientation of the mean force coefficient ($\bar{C}_L = 1.39$, inclined at 10.3° with respect to vertical) closely match values measured on tethered flies (14, 15). The instantaneous forces are roughly normal to the surface of the wing at all times, indicating that at this Reynolds number, pressure forces dominate the shear viscous forces acting parallel to the wing (Fig. 1C). The records show a transient peak in aerodynamic force at the start and end of each upstroke and downstroke (Fig. 1, D and E). The timing of these force transients relative to stroke reversal suggests that they result from some undetermined rotational effect and not from a translational mechanism such as delayed stall.

Translational forces. In order to test more rigorously whether rotational mechanisms were responsible for the two force peaks straddling stroke reversal, we estimated the forces that are generated solely by translation (Fig. 2). We calculated mean translational force coefficients (C_L and C_D) from data obtained by moving the wing through a 180° arc at constant velocity and fixed angle of attack (14). To obtain a representative mean value, we averaged the measured force coefficients over the interval indicated by the dotted lines in Fig. 2A. The values of the resulting translational lift and drag coefficients are consistent with similar measurements made on a two-dimensional (2D) model wing at an identical Reynolds number (7). The force coefficients of the 3D wing are slightly smaller than the maximum transient values generated by a 2D wing, but larger than the 2D steady-state values (Fig. 2D). These results confirm the important contribution of delayed stall in lift production during the translational portion of the wing stroke. The observation that the 3D force coefficients are lower than the 2D peak transient values, but higher than the 2D steady-state values, is entirely consistent with the flow patterns generated during force production. Whereas wing motion in 2D gives rise to an alternating pattern of unstable vortices termed a “von Kármán street” (7), the leading edge vortex generated by the 3D model fly wing was stable throughout motion (16). The stability of the flow structure is manifest as constant force generation during translation (Fig. 2, A and B), in marked contrast to the 2D case (7). Thus, as has been previously suggested, axial flow along the length of the wing appears to stabilize the leading edge vortex throughout translation (5, 11). Where-

¹Department of Integrative Biology, University of California, Berkeley, CA 94720, USA. ²Theodor-Boveri-Institute, Department of Behavioral Physiology and Sociobiological Zoology, University of Würzburg am Hubland, 97074 Würzburg, Germany.

*To whom correspondence should be addressed. E-mail: flymanmd@socrates.berkeley.edu

as axial flow stabilizes force production at a level greater than that possible under steady-state conditions in 2D, the loss of energy from the vortex core probably limits force generation below the maximum 2D level.

The stability of the force coefficients following an impulsive start justifies the attempt to reconstruct a “quasi-steady” estimate of

translational forces based on stroke kinematics. The results of such predictions for *Drosophila* kinematics are shown in Fig. 1, D and E. The calculations do not account for delays in the development of force via the Wagner effect (17) and probably represent a slight overestimate of the translational component. Although the translational values closely

match the magnitude of the measured force near the middle of each half-stroke, they do not accurately predict the forces during stroke reversal. One potential artifact in the measurements of aerodynamic forces during stroke reversal is the contamination by inertial forces due to the linear and angular acceleration of the wing. However, a series of

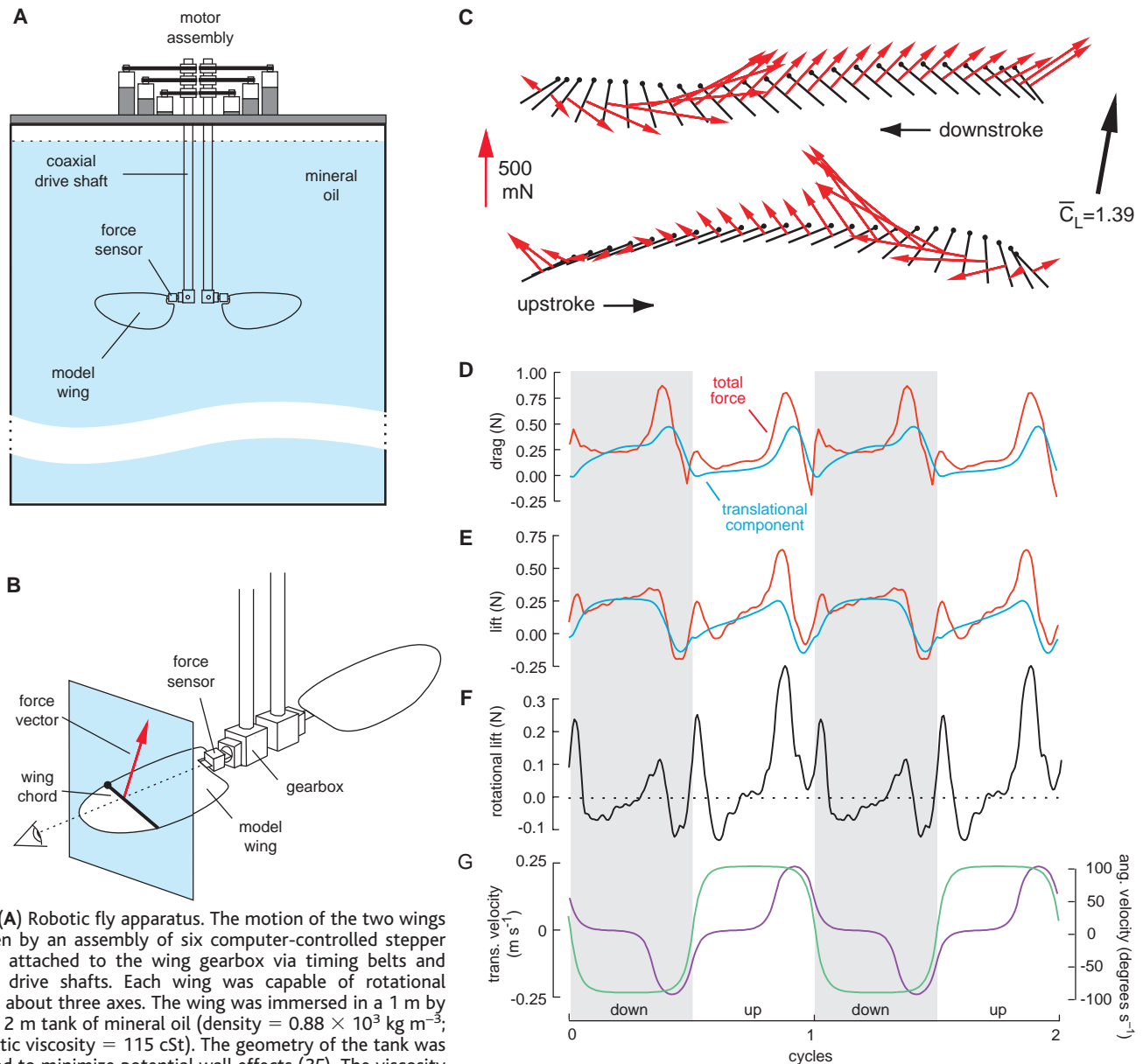


Fig. 1. (A) Robotic fly apparatus. The motion of the two wings is driven by an assembly of six computer-controlled stepper motors attached to the wing gearbox via timing belts and coaxial drive shafts. Each wing was capable of rotational motion about three axes. The wing was immersed in a 1 m by 1 m by 2 m tank of mineral oil (density = $0.88 \times 10^3 \text{ kg m}^{-3}$; kinematic viscosity = 115 cSt). The viscosity of the oil, the length of the wing, and the flapping frequency of the model were chosen to match the Reynolds number (Re) typical of *Drosophila* ($Re = 136$). The 25-cm-long model wings were constructed from Plexiglas (3.2 mm thick) cut according to the planform of a *Drosophila* wing (26). The base of one wing was equipped with a 2D force transducer consisting of two sets of strain gauges wired in full-bridge configuration (27). **(B)** Close-up view of robotic fly. In Figs. 1, 3, and 5, measured forces are plotted as vectors superimposed over wing chords inclined at the instantaneous angle of attack. The vectors and wing chords are drawn as if viewed from a line of sight that runs axially along the length of the wing. **(C)** Diagram of wing motion indicating magnitude and orientation of force vectors generated throughout the stroke by a kinematic pattern based on *Drosophila* (stroke amplitude = 160° ; frequency = 145 mHz; angle of attack at

midstroke = 20° upstroke, 40° downstroke). Black lines indicate the instantaneous position of the wing at 25 temporally equidistant points during each half-stroke. Small circles mark the leading edge. Time moves right to left during downstroke, left to right during upstroke. Red vectors indicate instantaneous flight forces. The large black vector at the right indicates the orientation of the mean force coefficient. **(D and E)** The time history of lift and drag forces. The measured forces are plotted in red, and forces predicted from translation force coefficients are plotted in blue (see text and Fig. 2). Data are plotted over two stroke cycles, with downstroke indicated by gray background. **(F)** Time course of rotational lift, defined as the difference between measured and estimated translational values of lift. **(G)** Translational (green) and rotational (purple) velocities of the wing.

control experiments indicated that the forces generated during stroke reversal could not be explained by either translational or rotational inertia (18). To provide a rough time course of rotational effects we subtracted the translational prediction of lift from the measured value (“rotational lift,” Fig. 1F). The subtraction reveals two clear force peaks bracketing each stroke reversal. For the *Drosophila* kinematics shown in Fig. 1, rotational effects contribute roughly 35% of the total lift production throughout the stroke—a high value considering the brief duration over which they act.

Rotational circulation. The presence of two rotational force peaks separated in time suggests that they might represent distinct aerodynamic mechanisms. One possible explanation for the force peak at the end of each half-stroke is that the wing’s own rotation serves as a source of circulation to generate an upward force (6, 19). This mechanism, rotational circulation, is akin to the Magnus effect, which makes a spinning baseball curve from its path toward the plate (20). The surface of a rotating ball pulls air within the boundary layer as it spins, thus serving as a source of circulation. As the ball moves through the air, this circulation will increase the total flow velocity on one side and decrease it on the other. If the velocity is higher on the top, as in the case of backspin, the ball is pulled upward by the lower pressure. In the case of topspin, the net velocity is higher below and the ball is pulled downward. If a flapping wing generates lift via a mechanism similar to the Magnus effect, then the orientation of the resulting force should also depend critically on the direction of wing rotation. To adopt the proper angle of attack for each translational phase, the wing must pronate before the downstroke and supinate before the upstroke (see wing sections in Figs. 1C and 3E). If the wing flips early, before reversing direction, then the leading edge rotates backward relative to translation

(“backspin”) and should produce an upward component of lift. If the wing flips late, after reversing direction, then the leading edge rotates forward relative to translation (“topspin”) and should create a downward force. If the process of rotation spans the end of one

half-stroke to the beginning of the next, then the wing will generate first an upward force and then, following stroke reversal, a downward force. These predictions were verified by systematically changing the phase between wing translation and wing rotation in a

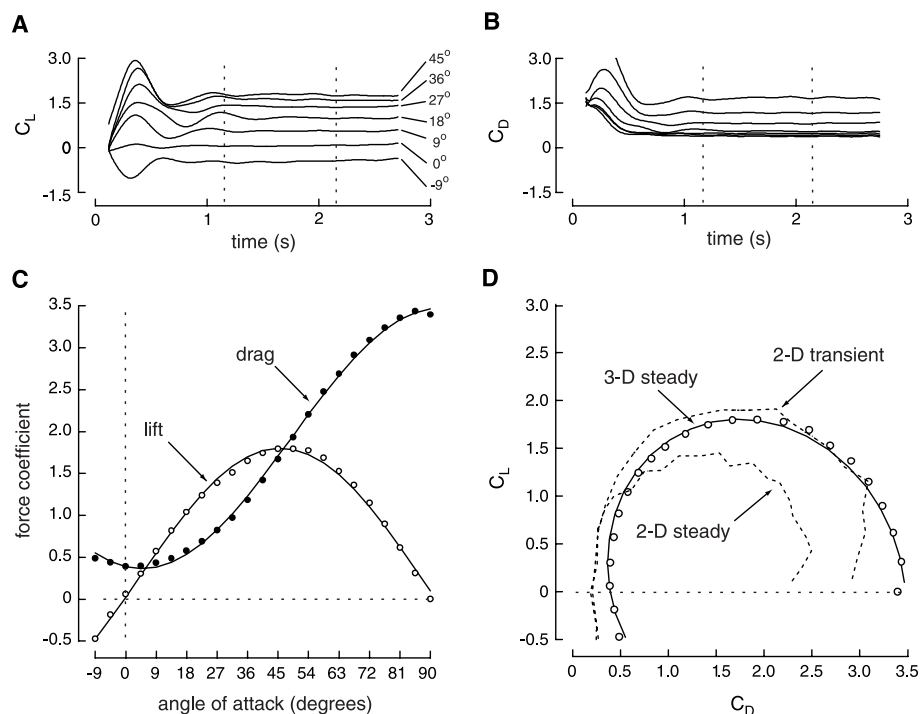
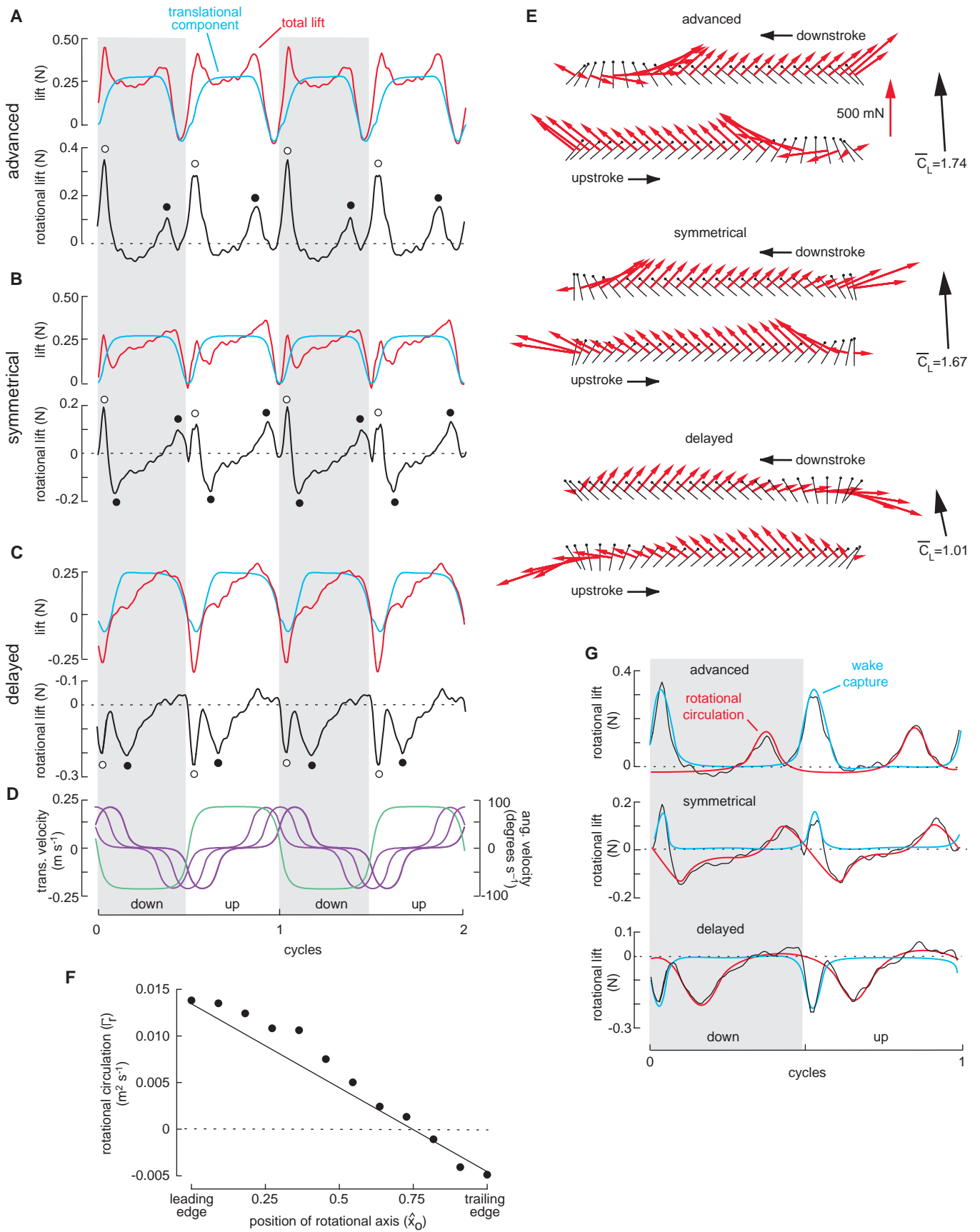


Fig. 2. Measurement of translational force coefficients. In each trial, we rapidly accelerated the wing from rest to a constant tip velocity of 0.25 m s^{-1} . The angle of attack was increased between trials in 4.5° increments. (A and B) The time history of lift (C_L) and drag (C_D) coefficients. Data are shown for seven different angles of attack, as indicated by the labels to the right of the traces in (A). Each trace begins with a large inertial transient caused by the rapid acceleration of the wing at the start of translation. After the inertial forces decay, the force trajectories are stable throughout translation. The dotted lines indicate the interval over which the values were averaged to calculate the mean values that were used to construct the relationships shown in (C) and (D). (C) Average translational force coefficients as a function of angle of attack. The two sets of data are well fit by simple harmonic relationships: $C_L = 0.225 + 1.58\sin(2.13\alpha - 7.20)$, $C_D = 1.92 - 1.55\cos(2.04\alpha - 9.82)$, where α = angle of attack. These formulas are used throughout the paper to estimate the translation component of flight force. (D) Polar representation of translational force coefficients and comparison with 2D measurements at a comparable Reynolds number (7). The influence of induced drag on the 3D wing is manifest by the small right shift of the curve relative to the 2D data.

Fig. 3 (opposite). Effects of rotational timing on lift generated using simplified stroke kinematics. In (A) through (C), the red trace indicates measured lift, and the blue trace represents the estimated translational component. Rotational circulation is the difference between the measured and predicted values. White dots indicate lift transients attributed to wake capture; black dots indicate transients attributed to rotational circulation. (A) Wing rotation precedes stroke reversal by 8% of the wingbeat cycle. (B) Wing rotation occurs symmetrically with respect to stroke reversal. (C) Wing rotation is delayed with respect to stroke reversal by 8% of the stroke cycle. (D) Translational (green) and rotational (purple) velocities for the experiments plotted in (A) through (C). Only the timing of wing rotation varied among all three cases. (E) Instantaneous force vectors superimposed on a diagram of wing motion for the three kinematic patterns (stroke amplitude = 160° , frequency = 145 mHz , angle of attack at midstroke = 40° for both upstroke and downstroke). Small differences ($\pm 4.5^\circ$) in upstroke and downstroke angles due to inaccuracies in wing alignment at the start of each trial result in slightly different force trajectories during upstroke and downstroke. The black vector to the right of each set of traces indicates the magnitude and orientation of the mean force coefficient. (F) Measured

values of rotational circulation are plotted as a function of the position of the rotational axis. The data were calculated using the total rotational force generated by the “advanced” kinematic pattern, close to the point of peak force generation (translational velocity at wing’s center of area = 0.15 m s^{-1} , angular velocity = $74 \text{ degrees s}^{-1}$). Each point represents a separate experiment in which the rotational axis of the wing was set at the value indicated by the abscissa. The straight line plots prediction based on thin airfoil theory (6, 20): $\Gamma_r = \pi\omega c^2(3/4 - \hat{x}_0)$, where Γ_r is total rotational circulation, ω is the instantaneous angular velocity of the wing, c is chord length, and \hat{x}_0 is the normalized position of the rotational axis. (G) Schematic representation of the proposed contribution of rotational circulation and wake capture. In the top three panels, measured values of rotational circulation (black lines) for the three kinematics conditions (advanced, symmetrical, and delayed rotation) are superimposed with functions drawn by eye to represent the hypothesized contribution of rotational circulation (red) and wake capture (blue). As described in the text, both the timing and polarity of rotational circulation depend on the phase of wing rotation. In contrast, rotation phase affects the polarity and magnitude, but not the timing of wake capture.



set of simplified wing kinematics (21) (see peaks labeled with black dots in Fig. 3, A through C). An advance in rotation relative to translation (Fig. 3, A and G) results in a positive lift peak at the end of each half-stroke, whereas a delay in rotation results in negative lift at the beginning of each half-stroke (Fig. 3, C and G). As predicted, symmetrical rotation causes a positive peak before and a negative peak after stroke reversal (Fig. 3, B and G). Thus, by properly adjusting the timing of wing rotation, an insect can generate lift via a rotational mechanism in excess of that produced by delayed stall.

The physics of rotating wings and baseballs differ in one important way, however: baseballs are round and insect wings are flat. This has two important consequences for the forces generated by rotational circulation. First, because pressure forces act at all times perpendicular to an object's surface, the rotational force on a wing will act normal to its chord, not perpendicular to the direction of motion as is the case with a spinning baseball (4). This influence is easily seen in the plots of the instantaneous force vector superimposed over the wing chord (Figs. 1C and 3E). As the angle of attack exceeds 90° , the force vector dips below the stroke plane and the sign of lift changes from positive to negative. Second, viscous forces within the air will make the flow above and below a flat wing fuse smoothly at the sharp trailing edge. This constraint, termed the Kutta condition, fixes a fluid stagnation point at the trailing edge of the wing. The functional consequence of the Kutta condition is that the amount of circulation and thus force produced by a rotating wing will depend critically upon the position of the rotational axis (6, 19). We confirmed this prediction by measuring total rotational circulation in a series of experiments in which we systematically varied the axis of rotation by changing the attachment point of the wing on the flapping apparatus (Fig. 3F). As predicted, rotational circulation decays as the axis of rotation is moved toward the trailing edge, changing sign at approximately three-fourths of a chord length from the leading edge of the wing. This result provides further evidence that force peaks generated during stroke reversal are due to rotational circulation.

Wake capture. Although rotational circulation can explain one of the stroke reversal forces, it cannot explain the large positive transient that develops immediately after the wing changes direction at the start of each half stroke (white dots, Fig. 3, A through C). These peaks are distinct from the rotational circulation peaks in that their timing is independent of the phase of wing rotation. One possible explanation for these forces is the mechanism of wake capture, in which the wing benefits from the shed vorticity of the

previous stroke. As has been demonstrated on 2D models of flapping insect wings, the flow generated by one stroke can increase the effective fluid velocity at the start of the next stroke and thereby increase force production above that which could be explained by translation alone (8). Because a significant portion of the fluid velocity that a wing encounters at the start of each stroke is due to the lingering wake, one clear prediction of the wake capture hypothesis is that a wing should continue to generate force at the end of a half-stroke even if it came to a complete stop. We tested this prediction by examining the time course of forces after halting wing motion at the end of the upstroke. As shown in Fig. 4, the wing generates force for several hundred milliseconds following the end of translation. The

time course of this posttranslational force is similar to that of the force transients at the start of each half-stroke during continuous flapping. The flow visualizations made immediately before stroke reversal reveal peak-induced velocities that are comparable to the maximum translational velocity of the wing, and of sufficient magnitude to generate the observed forces after the wing changes direction (Fig. 4B).

Whereas the timing of the wake capture force is constant, its magnitude and direction depend on the phase relationship between rotation and translation (Fig. 4, A and B). If rotation precedes stroke reversal, the wing intercepts its own wake so as to generate positive lift. If rotation is delayed until the start of the downstroke, then the flow intercepts

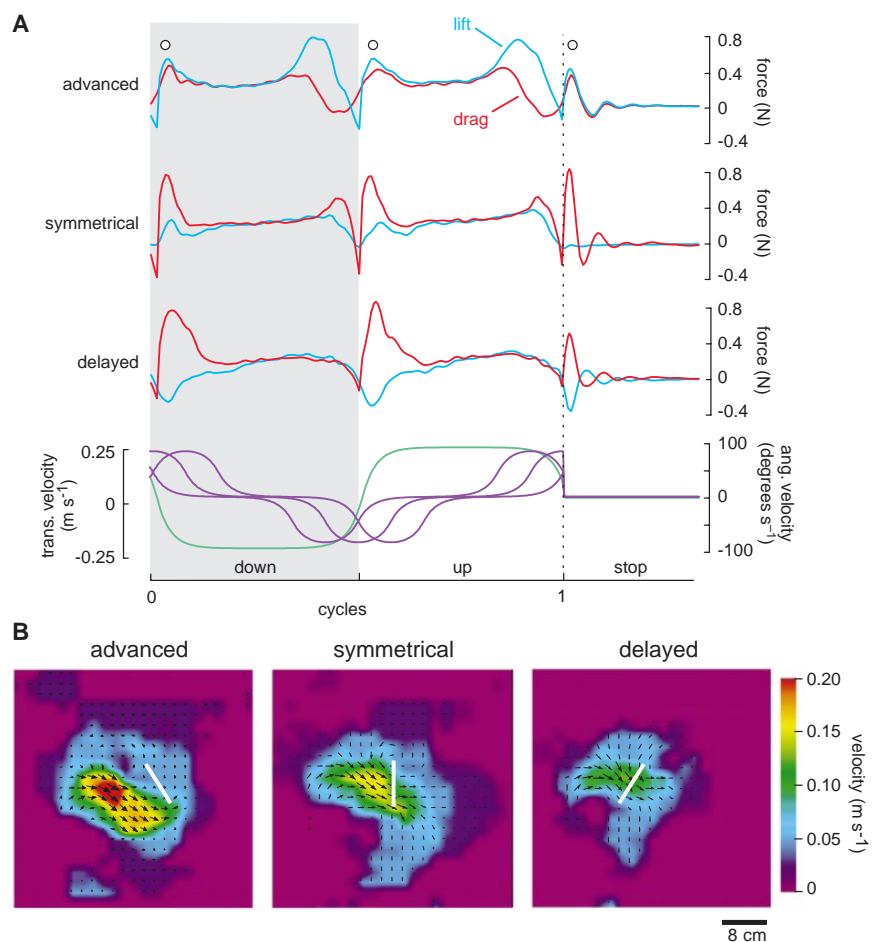


Fig. 4. Evidence for wake capture at the end of each half-stroke. (A) Lift (red) and drag (blue) are plotted for one continuous cycle preceding a complete stop at the end of the upstroke. When wing rotation is advanced, the wing develops lift and drag after translation has ceased. When wing rotation is symmetrical and stops in a vertical position, the posttranslation force is pure drag with no lift component. When rotation is delayed, the wing generates negative lift at the end of translation. The rising phase of the posttranslational transients is similar to that of the force transients at the start of each half-stroke during continuous flapping (white dots). (B) Flows through the midchord of the wing (white bar) immediately before a complete stop. Arrow lengths and direction indicate magnitude and orientation of local fluid velocity. Fluid velocity is also indicated by pseudocolor background. Although the gross orientation of the flow is similar in all three cases, the flow velocities are greater when rotation is advanced, consistent with the occurrence of stronger rotational circulation generated and subsequently shed during the upstroke. The flow images were generated by particle image velocimetry (16).

the wing at an angle that produces negative lift. With symmetrical rotation, the wing has a 90° angle of attack at the midpoint of stroke reversal and produces no lift (but high drag) if stopped at the end of the upstroke. Figure 4B also shows that the peak velocities in the near wake are much greater when rotation is advanced relative to stroke reversal. This result is expected because the rotational circulation generated at the end of the previous half-stroke is greater under these conditions, resulting in stronger vorticity shed within the wake. Collectively, the combined effect of wake strength and the starting angle of attack explains why, during continuous flapping, the lift peaks caused by wake capture are large and positive if rotation is advanced, small and positive if rotational is symmetrical, and small and negative if rotation is delayed (Fig. 3, A through C, and G). The increased magnitude of the wake capture force following a prominent rotational

circulation effect underscores a remarkable feature of the wake capture mechanism: the animal's ability to extract energy from its own wake. In general, wakes are a manifestation of the energy lost to the external medium by a moving object. By rapidly changing direction at the end of each translational phase, an insect wing can recover energy from the air that was lost during the previous stroke, greatly improving the overall efficiency of force production.

Rotational forces and flight control.

Any general theory of insect flight aerodynamics needs to explain not only how animals produce enough lift to stay in the air, but also how they can modulate flight forces during steering maneuvers. The results we describe indicate that rotational circulation and wake capture, though distinct phenomena, nevertheless interact synergistically in a way that makes them useful mechanisms for

controlling aerodynamic forces. An advance in wing rotation not only generates circulatory forces at the end of each stroke, it also increases the strength of the wake and ensures that the wing has the proper orientation to use the shed vorticity for generating positive lift at the start of the next stroke. As a consequence of this synergy, flight force is exquisitely sensitive to the phase of wing rotation. A phase advance of 8% (from the “delayed” to “symmetrical” conditions of Fig. 3) increases the mean lift coefficient by 67% (Fig. 3F). In contrast, the mean lift coefficient predicted from translational mechanisms does not change with the timing of wing rotation. This sensitivity of the forces to rotational timing is consistent with the kinematic changes exhibited by *Drosophila* during steering behaviors. During visually induced maneuvers, flies advance the timing of supination on the wing outside of a turn and delay supination on the wing inside of a turn (22). According to the above results, this alteration would help to generate the required change in yaw torque. By advancing the timing of rotation on both wings, a fly could generate the symmetrical increase in force required for forward or upward acceleration.

A general theory of insect flight. The ability to explain general phenomena determines the ultimate utility of any theory in biology. Are these results based on the kinematics of small flies applicable to other insects? Although our impression of insect diversity is strongly influenced by animals large enough to be noticeable, the length of the average insect is 4 to 5 mm, only slightly larger than *Drosophila* (23). Therefore, most insects operate within a Reynolds number regime that is similar to that of our robotic fly. However, the most rigorous test of our model is in its application to insects using radically different patterns of wing motion. The peculiar kinematics of hoverflies, often considered the most aerodynamically sophisticated of all insects (1), provide one such test. The stroke amplitude of hoverflies is quite small and the angular rotation of the wing is rapid. Using published data (13), we generated a series of kinematic patterns based on hoverfly wing motion. The forces generated by a simple hoverfly pattern consisting of symmetrical upstroke and downstroke motion are shown in Fig. 5. The discrepancy between measured forces and those predicted from translational force coefficients is especially large. The wing motion generates two distinct force peaks at the beginning and end of each half-stroke that are consistent with especially potent examples of rotational circulation and wake capture. Although our conclusions are limited by the fact that most hoverflies operate at a higher Reynolds number ($Re \approx 500$) than we are currently able to re-create ($Re \approx 140$), these animals would

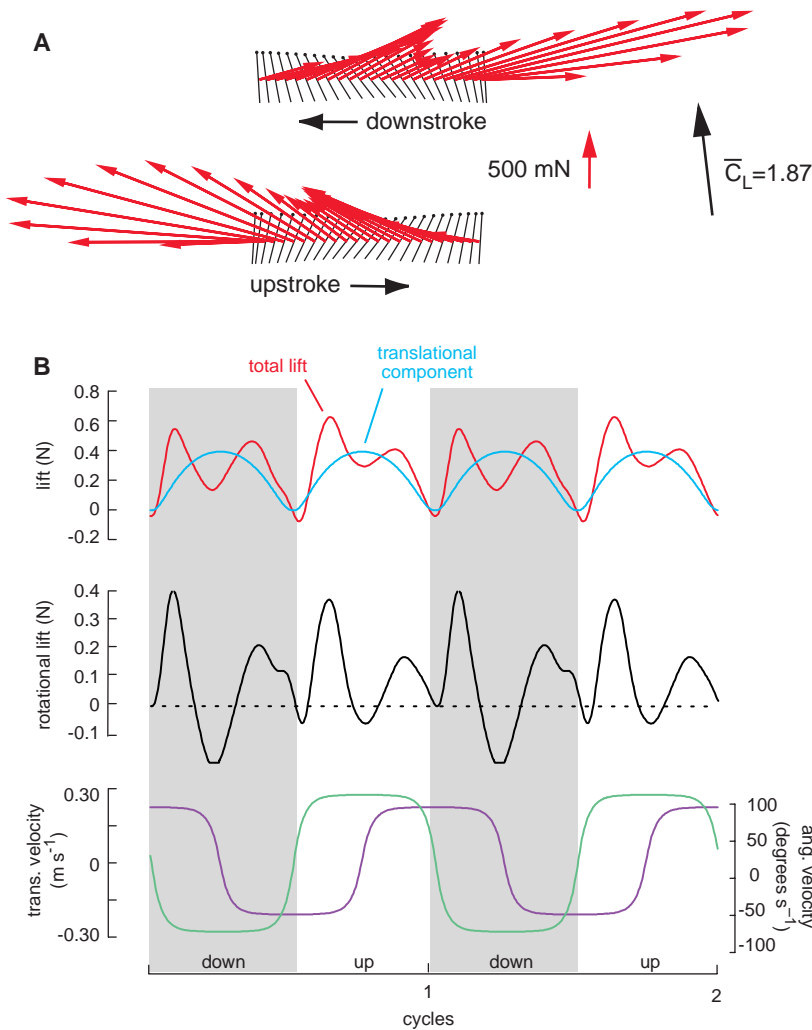


Fig. 5. Forces generated by a kinematic pattern based on the wing motion of hoverflies. (A) Instantaneous force vectors superimposed on a diagram of wing motion (stroke amplitude = 69°, frequency = 0.402 mHz, angle of attack at midstroke = 50° for both upstroke and downstroke). (B) Time history of measured rotational (red) and translational estimates (blue) of lift, rotational lift, and kinematic velocities. Translation (green) and rotational (purple) velocities are shown at bottom.

appear to make a more extensive use of rotational mechanisms than do fruit flies. In any event, this exercise indicates that while a theory of insect flight based purely on translation could not explain the complex time history of forces generated by hoverfly kinematics, the hoverfly pattern fits well within a more general model that incorporates both translational and rotational mechanisms.

In summary, direct measurements of the forces produced by flapping wings suggest that the aerodynamics of insect flight may be explained by the interaction of three distinct, yet interactive mechanisms: delayed stall, rotational circulation, and wake capture. Whereas delayed stall is a translational mechanism, rotational circulation and wake capture depend explicitly on the pronation and supination of the wing during stroke reversal. These findings are significant for several reasons. First, delayed stall is not sufficient alone to explain the elevated aerodynamic performance required for active flight in *Drosophila*. The rotational mechanisms we describe are necessary components of the basic unsteady aerodynamic toolkit in this species (24). Second, a more general theory of insect aerodynamics that incorporates both translational and rotational mechanisms shows promise in explaining the force-generating mechanisms of many species. As suggested by the forces generated by hoverfly kinematics, different insects may emphasize the translational and rotational mechanisms to different degrees. It will be of interest in the future to compare the relative energetic and aerodynamic efficiency of translationally and rotationally dominated kinematic patterns. Finally, the regulation of rotational phase provides insects with one of the most potent means of controlling flight forces during steering maneuvers. Thus, an understanding of rotational mechanisms provides a link between the unsteady aerodynamics and the behavior and neurobiology of flight control.

References and Notes

1. S. Dalton, *Borne on the Wind* (Reader's Digest Press, New York, 1975); T. S. Collett and M. F. Land, *J. Comp. Physiol. A* **99**, 1 (1975); W. Nachtigall, *Insects in Flight* (McGraw-Hill, New York, 1974).
2. C. P. Ellington, *Philos. Trans. R. Soc. London Ser. B* **305**, 1 (1984).
3. ———, in *Biological Fluid Dynamics*, C. P. Ellington and T. J. Pedley, Eds. (Company of Biologists, London, 1995), pp. 109–129.
4. M. Dickinson, *Am. Zool.* **36**, 537 (1996).
5. T. Maxworthy, *J. Fluid Mech.* **93**, 47 (1981); *Annu. Rev. Fluid Mech.* **13**, 329 (1981).
6. C. P. Ellington, *Philos. Trans. R. Soc. London Ser. B* **305**, 79 (1984).
7. M. H. Dickinson and K. G. Götz, *J. Exp. Biol.* **174**, 45 (1993).
8. M. H. Dickinson, *ibid.* **192**, 179 (1994).
9. T. Weis-Fogh, *ibid.* **59**, 169 (1973); G. R. Spedding and T. Maxworthy, *J. Fluid Mech.* **165**, 247 (1986).
10. J. Marden, *J. Exp. Biol.* **130**, 235 (1987).
11. C. Van den Berg and C. P. Ellington, *Philos. Trans. R. Soc. London Ser. B* **352**, 317 (1997); C. P. Ellington, C. Van den Berg, A. P. Willmott, A. L. R. Thomas, *Nature* **384**, 626 (1996); A. P. Willmott, C. P. Ellington, A. L. R. Thomas, *Philos. Trans. R. Soc. London Ser. B* **352**, 303 (1997).
12. M. Cloupeau, J. F. Devillers, D. Devezeaux, *J. Exp. Biol.* **80**, 1 (1979); M. H. Dickinson and K. G. Götz, *ibid.* **199**, 2085 (1996); P. J. Wilkin and M. H. Williams, *Physiol. Zool.* **66**, 1015 (1993).
13. J. M. Zanker, *Philos. Trans. R. Soc. London Ser. B* **327**, 1 (1990); C. P. Ellington, *ibid.* **305**, 41 (1984); A. R. Ennos, *J. Exp. Biol.* **142**, 49 (1989); F.-O. Lehmann, thesis, Eberhard-Karls-Universität Tübingen, Germany (1994).
14. Translational lift coefficients were calculated according to the following equation: $C_L = 2F_L / (\rho v^2 S) U^2$, where ρ = fluid density (880 kg m⁻³), $F_L^2(S)$ is the second moment of wing area (0.40), S is surface area (0.0167 m²), F_L is the measured lift force, and U is the path velocity of the wing tip. The drag coefficient, C_D , was calculated by similar means. The same formulae were used in reverse to predict the translational component of flight force for a given set of kinematics.
15. K. G. Götz and U. Wandel, *Biol. Cybernetics* **51**, 135 (1984).
16. To visualize the pattern of flow in the mineral oil, we forced air through a series of aquarium stones at the bottom of the tank. After a few large bubbles quickly rose, the remaining small, slowly rising bubbles generated a stable seed for both qualitative and quantitative analysis of the flow. To visualize a select section, we used fiber-optic pipes and pairs of black shutters to create thin slices of white light. For particle image velocimetry, images of bubble motion through a light slice were captured at 30 frames per second using a 0.5-inch diagonal chip CCD (charge-coupled device) camera. Flow fields were generated by finding maxima in 2D spatial cross-correlations of 40 pixel by 40 pixel windows from successive images. To reduce noise, adjacent windows overlapped by 50%. All software was written using MATLAB, version 5.2 (Mathworks, Inc.).
17. H. Wagner, *Z. Angew. Math. Mech.* **5**, 17 (1925).
18. Our calibration procedure using a dummy inertial wing automatically eliminates any contribution of wing mass acceleration and gravity from our measurements. However, the mass of fluid attached to the wing ("added mass") is a dynamic quantity that may change with speed and angle of attack and is thus difficult to model either physically or mathematically. In order to test whether rotational transients might be caused by the translational inertia of added mass, we repeated our experiments using a modified kinematic pattern in which the translation of the wing was limited to a flat stroke plane (Fig. 3). Under these conditions, added mass acceleration might contribute to an error in the measurement of drag, but it should not contaminate the measurement of the lift. As indicated in Fig. 3A, the two large lift transients are still present during stroke reversal when the wing is flapped using the simplified kinematic pattern, indicating that added mass accelerations cannot explain the rotational forces. In order to test whether our results were contaminated by rotational inertia, we rotated the model wing according to the same kinematic pattern used in the other experiments, but in the absence of translation. The forces generated by this purely rotational motion were negligible.
19. Y. C. Fung, *An Introduction to the Theory of Aeroelasticity* (Dover, New York, 1993).
20. R. K. Adair, *The Physics of Baseball* (Harper and Row, New York, 1990).
21. To better study rotational effects, we used a simplified kinematics pattern in which translational motion was limited to a flat stroke plane and the upstroke and downstroke angles were equal (18).
22. M. H. Dickinson, F.-O. Lehmann, K. G. Götz, *J. Exp. Biol.* **182**, 173 (1993).
23. R. M. May, in *Diversity of Insect Faunas*, L. A. Mound and N. Waloff, Eds., no. 9 of the *Symposia of the Royal Entomological Society of London Series* (Blackwell, New York, 1978), chap. 12, pp. 188–204.
24. *Drosophila* are known to use the clap and fling at the start of the downstroke [K. G. Götz, *J. Exp. Biol.* **128**, 35 (1987)]. Using the model fly, we measured a small (5 to 10%) increase in the mean lift produced during each cycle caused by this effect, which though significant, is small relative to the effects of delayed stall, rotational circulation, and wake capture.
25. At closest approach, the wing tip came within 22 cm of the top surface, 18 cm from the side walls, and 160 cm from the bottom of the tank. In order to test that the forces measured within the enclosed tank did not deviate from those expected in an infinite volume, we carefully mapped the change in force production with distance from the tank boundaries. In three separate sets of experiments, we moved the robotic apparatus incrementally toward each boundary and measured the forces generated by the *Drosophila* kinematic pattern shown in Fig. 1. The changes in mean lift coefficient with distance from the solid-liquid (side and bottom) and air-liquid (top) interfaces were closely approximated by exponential functions (x in meters): side, $C_L = 1.38 + 0.59e^{-33.1x}$; top, $C_L = 1.37 + 1.20e^{-25x}$; bottom, $C_L = 1.55e^{-21.7x} + 1.39(1 - e^{-12.8x})$. Thus, the forces generated by the wing at the center location fell within 1% of asymptotic values in all dimensions, indicating that the experimental conditions well approximate an infinite volume. It should be noted that in shortening the distance to the bottom of the tank, force production passed through a global minimum at a depth of 8 cm. The augmentation of lift at extremely low altitude is a manifestation of the ground effect, an interaction of a downward-directed wake with a solid boundary [J. M. V. Rayner, *Philos. Trans. R. Soc. London Ser. B* **334**, 119 (1991)].
26. High-speed video films indicate that *Drosophila* wings do not twist extensively during flight. However, to test for effects of wing flexion, we repeated experiments using a flexible composite wing consisting of a Plexiglas leading edge and a thin metal foil blade. The thickness of the foil was chosen to produce deformations comparable to those observed in real flies. The use of flexible wings did not significantly alter any of the findings, although forces measured with rigid wings were typically higher than those measured with flexible wings.
27. The sensor was a miniaturized version of a design used in a previous 2D study (7). One sensor measured total force normal to the surface of the wing, while the other measured the force parallel to the surface in the chordwise direction. Preliminary experiments indicated that lengthwise parallel forces were negligible compared to the other components and have been ignored. Lift and drag forces, defined conventionally with respect to wing motion, were constructed trigonometrically from the normal and parallel channels. We deliberately designed the sensor to measure shear deflection and not cantilever bending so that measurements would not be sensitive to the loading distribution on the wing. Forces measured with calibration weights placed at the base, tip, trailing edge, and leading edge of the wing differed by <5%. The final calibration was based on static loading at the wing's center of area. During data collection, we used a low-pass four-pole Bessel filter with a cut-off frequency of 10 Hz, roughly 50 times the flapping frequency. Spectral analysis indicated that this filter introduced no appreciable phase lag within the range of relevant frequencies. During subsequent offline analysis, we conditioned each signal using an 8-pole recursive digital filter (Butterworth) with a cut-off of 5 Hz and zero phase delay (implemented in MATLAB, Mathworks, Inc.). Each trial consisted of a burst of four continuous wing strokes; four such bursts were averaged for each experimental condition. Force measurements during the first cycle of each burst were slightly different due to transient effects and have been excluded from the present analysis. Each experiment was repeated using an inertial model, consisting of a short brass cylinder machined to have an equal mass and center of mass to that of the wing. The data from the inertial model were subtracted from the raw wing data to remove the contributions of wing inertia and gravity.
28. Supported by grants from NSF (IBN-9723424), Defense Advanced Research Projects Agency, and the U.S. Office of Naval Research (M.H.D.).

25 January 1999; accepted 7 April 1999